

Progress in phosphors and filters for luminescent solar concentrators

Dick K. G. de Boer,^{1,2,*} Dirk J. Broer,² Michael G. Debije,² Wilco Keur,¹
Andries Meijerink,³ Cees R. Ronda,^{1,3} and Paul P. C. Verbunt²

¹Philips Research, High Tech Campus 4, 5656 AE Eindhoven, The Netherlands

²Functional Organic Materials and Devices, Eindhoven University of Technology, Box 513, 5600 MB Eindhoven, The Netherlands

³Condensed Matter and Interfaces, Debye Institute for Nanomaterials Science, Utrecht University, Princetonplein 5, 3584 CC Utrecht, The Netherlands

*dick.de.boer@philips.com

Abstract: Luminescent solar concentrators would allow for high concentration if losses by reabsorption and escape could be minimized. We introduce a phosphor with close-to-optimal luminescent properties and hardly any reabsorption. A problem for use in a luminescent concentrator is the large scattering of this material; we discuss possible solutions for this. Furthermore, the use of broad-band cholesteric filters to prevent escape of luminescent radiation from this phosphor is investigated both experimentally and using simulations. Simulations are also used to predict the ultimate performance of luminescent concentrators.

©2012 Optical Society of America

OCIS codes: (350.6050) Solar energy; (160.2540) Fluorescent and luminescent materials.

References and links

1. G. Smestad, H. Ries, R. Winston, and E. Yablonovitch, "The thermodynamic limits of light concentrators," *Sol. Energy Mater.* **21**(2-3), 99–111 (1990).
2. J. M. Castro, D. Zhang, B. Myer, and R. K. Kostuk, "Energy collection efficiency of holographic planar solar concentrators," *Appl. Opt.* **49**(5), 858–870 (2010).
3. R. Winston, J. C. Minano, and P. Benitez, *Nonimaging optics* (Elsevier Academic Press, 2005).
4. T. M. de Jong, D. K. G. de Boer, and C. W. M. Bastiaansen, "Surface-relief and polarization gratings for solar concentrators," *Opt. Express* **19**(16), 15127–15142 (2011).
5. D. K. G. de Boer, "Luminescent and non-luminescent solar concentrators: challenges and progress," *Renewable Energy and the Environment 2011* (Optical Society of America, Washington, DC, 2011), SRTb6.
6. W. H. Weber and J. Lambe, "Luminescent greenhouse collector for solar radiation," *Appl. Opt.* **15**(10), 2299–2300 (1976).
7. A. Goetzberger and W. Greube, "Solar-energy conversion with fluorescent collectors," *Appl. Phys. (Berl.)* **14**(2), 123–139 (1977).
8. E. Yablonovitch, "Thermodynamics of the fluorescent planar concentrator," *J. Opt. Soc. Am.* **70**(11), 1362–1363 (1980).
9. U. Rau, F. Einsele, and G. C. C. Glaeser, "Efficiency limits of photovoltaic fluorescent collectors," *Appl. Phys. Lett.* **87**(17), 171101 (2005).
10. P. P. C. Verbunt, A. Kaiser, K. Hermans, C. W. M. Bastiaansen, D. J. Broer, and M. G. Debije, "Controlling light emission in luminescent solar concentrators through use of dye molecules aligned in a planar manner by liquid crystals," *Adv. Funct. Mater.* **19**(17), 2714–2719 (2009).
11. M. G. Debije, M. P. Van, P. P. C. Verbunt, M. J. Kastelijn, R. H. L. van der Blom, D. J. Broer, and C. W. M. Bastiaansen, "Effect on the output of a luminescent solar concentrator on application of organic wavelength-selective mirrors," *Appl. Opt.* **49**(4), 745–751 (2010).
12. D. K. G. de Boer, C.-W. Lin, M. P. Giesbers, H. J. Cornelissen, M. G. Debije, P. P. C. Verbunt, and D. J. Broer, "Polarization-independent filters for luminescent solar concentrators," *Appl. Phys. Lett.* **98**(2), 021111 (2011).
13. D. K. G. de Boer, "Optimizing wavelength-selective filters for luminescent solar concentrators," *Proc. SPIE* **7725**, 77250Q, 77250Q-9 (2010).
14. L. R. Wilson, B. C. Rowan, N. Robertson, O. Moudam, A. C. Jones, and B. S. Richards, "Characterization and reduction of reabsorption losses in luminescent solar concentrators," *Appl. Opt.* **49**(9), 1651–1661 (2010).
15. K. Barnham, J. L. Marques, J. Hassard, and P. O'Brien, "Quantum-dot concentrator and thermodynamic model for the global redshift," *Appl. Phys. Lett.* **76**(9), 1197–1199 (2000).
16. R. Reisfeld and Y. Kalisky, "Improved planar solar converter based on uranyl neodymium and holmium glasses," *Nature* **283**(5744), 281–282 (1980).

17. J. Zubia and J. Arrue, "Plastic optical fibers: An introduction to their technological processes and applications," *Opt. Fiber Technol.* **7**(2), 101–140 (2001).
18. C. R. Ronda, S. de Brouwer, W. Keur, D. K. G. de Boer, A. Meijerink, A. J. J. Bos, and P. Doorenbos, "Luminescence of Sm^{2+} in strontium borates and aluminosilicates," to be published (2012).
19. C. Kulshreshtha, S. H. Cho, Y. S. Jung, and K.-S. Sohn, "Deep red color emission in an Sm^{2+} -doped SrB_4O_7 phosphor," *J. Electrochem. Soc.* **154**(3), J86–J90 (2007).
20. C. Ronda, *Luminescence: From Theory to Applications* (Wiley, 2008).
21. R. Mehra, "Application of refractive index mixing rules in binary systems of hexadecane and heptadecane with n-alkanols at different temperatures," *Proc. Indiana Acad. Sci. (Chem. Sci.)* **115**(2), 147–154 (2003).
22. Y. S. Oseledchik, A. L. Prosvirnin, A. I. Pisarevskiy, V. V. Starshenko, V. V. Osadchuk, S. P. Belokryz, N. V. Svitanko, A. S. Korol, S. A. Krikunov, and A. F. Selevich, "New nonlinear optical crystals: strontium and lead tetraborates," *Opt. Mater.* **4**(6), 669–674 (1995).
23. Y. Wang, T. Flaim, R. Mercado, S. Fowler, D. Holmes, and C. Planje, "Hybrid high refractive index polymer coatings," *Proc. SPIE* **5724**, 42–49 (2005).
24. Titanium dioxide P25 (Degussa, Evonik Industries).
25. Y. Paz, "Application of TiO_2 photocatalysis for air treatment: Patents' overview," *Appl. Catal. B* **99**(3-4), 448–460 (2010).
26. Narec Solar, <http://narecsolar.com/>
27. L. Desmet, D. K. G. de Boer, A. J. M. Ras, H. Zahn, M. G. Debije, S. Tsoi, P. P. C. Verbunt, C. W. M. Bastiaansen, and D. J. Broer, "Monocrystalline silicon luminescent solar concentrator with 4.2% conversion efficiency," to be published (2012).
28. M. Peters, J. C. Goldschmidt, P. Löper, B. Bläsi, and A. Gombert, "The effect of photonic structures on the light guiding efficiency of fluorescent concentrators," *J. Appl. Phys.* **105**(1), 014909 (2009).
29. D. J. Broer, G. N. Mol, J. A. M. M. van Haaren, and J. Lub, "Photo-induced diffusion in polymerizing chiral-nematic media," *Adv. Mater. (Deerfield Beach Fla.)* **11**(7), 573–578 (1999).
30. N. P. M. Huck, I. Staupe, A. Thirouard, and D. K. G. de Boer, "Light polarization by cholesteric layers," *Jpn. J. Appl. Phys.* **42**(Part 1, No. 8), 5189–5194 (2003).
31. D.K.G. de Boer, D.J. Broer, C.R. Ronda, and H.J. Cornelissen, "Luminescent solar concentrator," WO 2011/064691 A2.
32. http://www.opticalres.com/lt/ltprodds_f.html
33. S.-J. Chang, W.-S. Liao, C.-J. Ciou, J.-T. Lee, and C.-C. Li, "An efficient approach to derive hydroxyl groups on the surface of barium titanate nanoparticles to improve its chemical modification ability," *J. Colloid Interface Sci.* **329**(2), 300–305 (2009).

1. Introduction

In light-guide based solar-concentrator systems, sunlight is coupled into a plate and then guided towards small photovoltaic cells by total internal reflection (TIR). Such devices are attractive, since they are inexpensive and thin and can be easily integrated in appliances. There are several ways to couple sunlight into a light guide [1]: non-luminescent (scattering, refraction or diffraction [2]) and luminescent. Non-luminescent concentrators suffer from limitations given by conservation of étendue [3]. In the case of diffuse light and/or non-tracking systems, the maximum attainable concentration equals n^2 , where n is the refractive index of the light-guide material. In the case of direct sunlight, only a limited angular part of the sky has to be covered and the attainable concentration will be higher [4,5].

Luminescent solar concentrators (LSCs) [6,7] do not suffer from this limitation. In an LSC, incident short-wavelength light is converted by a luminescent material into longer-wavelength light, which is guided towards the photovoltaic cells. If the energy difference between the incident short-wavelength and emitted long-wavelength light is $\Delta E = E_{\text{in}} - E_{\text{out}}$, the maximum attainable concentration equals $n^2 (E_{\text{out}} / E_{\text{in}})^2 \exp(\Delta E/kT)$, where T is the temperature of the concentrator [1,8]. The heat ΔE generated in the luminescence process can be exploited to lower the entropy of the light by an amount $\Delta E/T$, concentrating the light.

The underlying concept of the device can be understood by comparing a scattering and a luminescent concentrator, as shown in Fig. 1 (where, in all cases, a perfect mirror at the bottom of the device is assumed to prevent light escaping from the bottom). In the scattering concentrator of Fig. 1(a), the incident light is scattered by a scattering layer. Part of the scattered light escapes, but a substantial part will stay in the light guide. However, if the light guide is long, this light will reencounter the scattering layer and has a significant chance to escape. For this reason, the attainable concentration of a scattering concentrator is limited. In the luminescent concentrator of Fig. 1(b), the incident light is absorbed by the luminescent layer and converted into light of longer wavelength. Part of this luminescent light escapes the

surfaces (unless additional measures are taken), but a substantial part will stay in the light guide. If the light reencounters the luminescent layer, it will continue to travel unimpeded, provided that the luminescent layer neither scatters the light nor reabsorbs it. In this case, the attainable concentration is high. If the luminescent layer is not perfect, it may have a certain amount of scattering and/or it may reabsorb the luminescent light, part of which may be subsequently reemitted, Fig. 1(c). One can improve upon the devices shown in Figs. 1(b) and 1(c), if the escaping luminescent light can be redirected into to the light guide. This can be achieved by applying a suitable wavelength-selective filter, which reflects the luminescent light but not the incident light that could be absorbed, Fig. 1(d). Note that such a filter would also work in the case of a reemitting or scattering luminescent layer. With a perfect wavelength-selective filter, in principle a very high concentration (of several thousands) can conceivably be achieved [9]. Another way to reduce escape losses, which we will not discuss further, is the use of directional emission by the luminescent material [10].

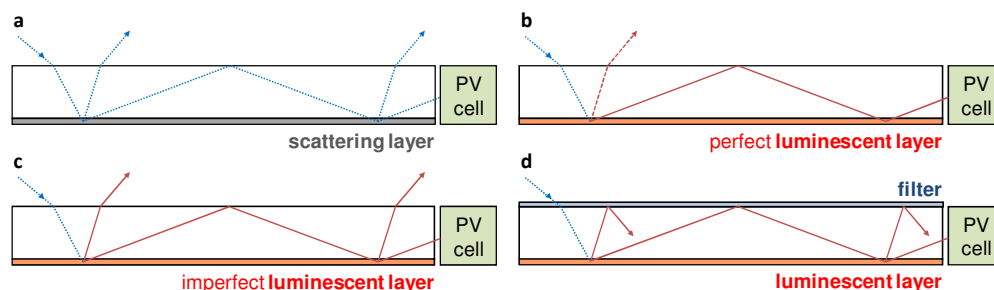


Fig. 1. (a) In a scattering concentrator, light initially in the light guide can escape by scattering. (b) In a luminescent concentrator, large part of the luminescent light stays inside the light guide. (c) If the luminescent material is not perfect, part of the luminescent light can escape. (d) A suitable wavelength-selective filter prevents escape of the luminescent light.

Considering the preceding discussion, the major challenges for designing an efficient LSC can be elucidated. First, a good luminescent material is needed. Apart from the normal requirements, such as good absorption and high quantum efficiency (QE), the luminescent material should also have low reabsorption. Even with a high QE, reabsorption and subsequent reemission (taking place in all directions) would result in escape of luminescent light. In Section 2, we will introduce a new luminescent material, an inorganic phosphor, which outperforms previous materials in this respect. A next requirement for an LSC is that the luminescent material should be applied in such a way that it does not scatter. This is not trivial for inorganic phosphors and in Section 3 this will be discussed further. Furthermore, it will be interesting to have good wavelength-selective filters for LSCs. Cholesteric liquid crystals are very well suited for this [11,12], as will be discussed in Section 4. If perfect filters were available, scatter and reemission would not be a problem. However, there are both theoretical and practical limits to what can be achieved in this respect. In a previous paper [13], we discussed how simulations help to find the required filter properties for absorption and reemission. In Section 5, we will present new results of simulations that show the influence of scatter and reabsorption, as well as what can be achieved by applying filters. In Section 6, we will conclude with the prospects for LSC technology.

2. New phosphor for LSC

The main drawbacks of luminescent materials that are being investigated for LSCs, including organic dyes [14] and quantum dots [15] is that they suffer from reabsorption as a result of significant overlap between their absorption and emission spectra. In this respect, rare-earth compounds are more promising, since in general they have large shifts between absorption and emission, whereas optical absorption between 4f levels is forbidden. However, both the inorganic phosphors [16] and the organo-metallic rare-earth complexes [14] investigated to date only absorb a limited part of the solar spectrum. If considering the optimal phosphor

properties, one has to realize that these will be a compromise, since small reabsorption implies a large spectral shift between absorption and emission, which means that the absorption spectrum cannot extend too far into long wavelengths. Furthermore, if the light guide is made from a common polymer like polymethylmethacrylate (PMMA) or polycarbonate, one must take into account that these materials demonstrate strong absorption [17] above 850 nm due to C-H vibrational overtones. Hence, the optimal phosphor [13] used with such light guides will show a narrow emission around 800 nm and have a broad absorption spectrum extending from the UV until approximately 100 nm below the onset of the emission spectrum.

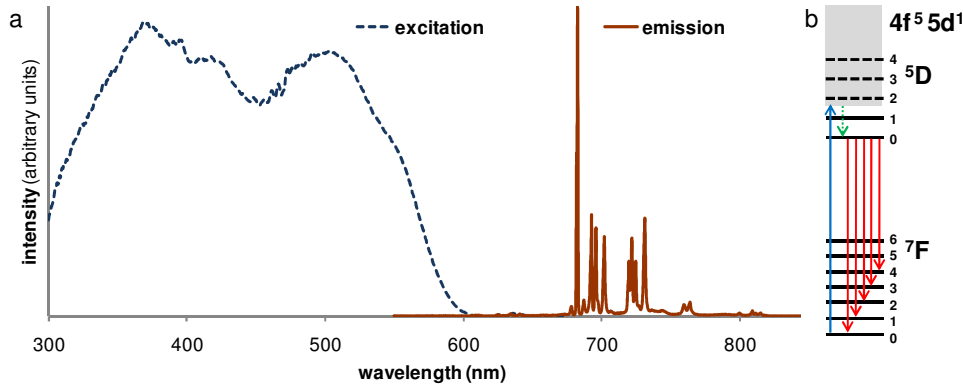


Fig. 2. (a) Excitation (at emission wavelength 685 nm) and emission spectrum (at excitation wavelength 500 nm) of $\text{SrB}_4\text{O}_7:5\%\text{Sm}^{2+},5\%\text{Eu}^{2+}$. (b) Energy levels and transitions for Sm^{2+} .

We have found that phosphors based on Sm^{2+} match most of these requirements. As is shown schematically in Fig. 2(b), absorption takes place from the 4f ground state to the 5d band. The location of the bottom of the 5d band, relative to the lowest 5D level is very important for the optical properties [18]. For use in an LSC, the situation in which the bottom of the 5d band is located not too close to the lowest 5D level is most interesting. In that case, non-radiative relaxation into the 5D levels may occur (Fig. 2(b), dashed line), followed by line emission. In view of the forbidden character, reabsorption in the corresponding transitions is weak. This situation occurs for Sm^{2+} in a SrB_4O_7 matrix. In Fig. 2(a), the absorption and emission spectra for this material are shown. The absorption spectrum is broad, whereas the emission spectrum consists of a main peak [19] at 685 nm and some smaller peaks extending up to 820 nm. Although the main emission line is at a somewhat shorter wavelength than preferable for an LSC (see above), this is the best phosphor system we found.

It was reported before [19] that in this system Eu^{2+} needs to be introduced for appreciable absorption and emission. A possible explanation is that, without Eu, part of the Sm is present as Sm^{3+} . When the europium concentration is sufficiently high, the Sm^{3+} concentration is strongly reduced and only Sm^{2+} emission is observed [18]. We found that good results are obtained if equal amounts of europium and samarium are used. As can be seen in Fig. 2(b), no appreciable emission from Eu^{2+} , Eu^{3+} or Sm^{3+} is present. Absorption by Eu^{2+} is expected to be followed by efficient energy transfer to Sm^{2+} in view of the high Sm^{2+} concentration.

We prepared $\text{SrB}_4\text{O}_7:5\%\text{Sm}^{2+},5\%\text{Eu}^{2+}$ by mixing appropriate amounts of SrCO_3 , Sm_2O_3 , Eu_2O_3 and excess H_3BO_3 , first firing this mixture first at 800 °C in air, then at 935 °C in a CO atmosphere, followed by dissolving the excess of boron oxide in water. The material was milled down to a particle size of approximately 5 μm . The absorption (excitation) and emission spectra of this material are shown in Fig. 2(a). The emission lines at 685 nm, 695 nm, 720 nm and 770 nm are due to the $^5\text{D}_0 \rightarrow ^7\text{F}_0$, $^5\text{D}_0 \rightarrow ^7\text{F}_1$, $^5\text{D}_0 \rightarrow ^7\text{F}_2$ and $^5\text{D}_0 \rightarrow ^7\text{F}_3$ transitions of Sm^{2+} , respectively. The absorption coefficient at 500 nm wavelength is approximately 300 cm^{-1} ; at 685 nm it is approximately 0.1 cm^{-1} . We measured an external

quantum efficiency (for the emission range between 650 and 850 nm) of more than 90%. X-ray diffraction showed no presence of other phases in this material.

3. Application of phosphor on light guides

For use in an LSC, the phosphor must be applied on a light guide in such a way that luminescent light does not escape by scattering. For organic dyes, quantum dots and organo-metallic complexes, scattering plays a minor role, since the constituent particles are smaller than the wavelength of light. Unfortunately, it is not trivial to avoid scatter for inorganic phosphors, since the constituent particles are much larger. These phosphors can be applied as particles dispersed in a binder. In general, the phosphor and the binder have different refractive indices, causing scattering of light. One way of preventing scatter is by including the phosphor as nanoparticles. However, it is not easy to produce such nanophosphors and in general their quantum efficiency is low [20]. Another way of preventing scatter is by matching the refractive index of the binder to that of the phosphor. Actually, only the scatter of luminescent light needs to be low; it is even favorable for the LSC performance to have some scatter of incident light, since that will enhance its absorption length.

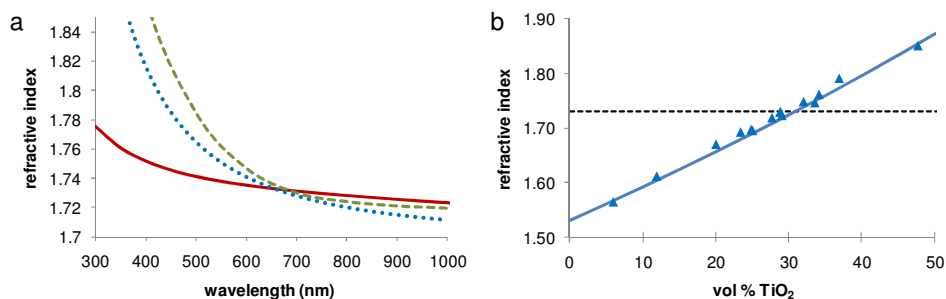


Fig. 3. (a) Refractive-index dispersion for SrB₄O₇ (solid line), high-index polyimide (dashed) and 29 volume% TiO₂ nanoparticles in organic binder (dotted). (b). Measured (triangles) and calculated [21] (solid line) refractive index at 685 nm for TiO₂ nanoparticles of various volume% dispersed in organic binder. Dashed line: index of SrB₄O₇.

In Fig. 3(a) the dispersion of the refractive index is shown for SrB₄O₇ (solid line, where the small birefringence [22] is within the line thickness) and some suitable binders. The index of SrB₄O₇ at the main Sm²⁺ emission line of 685 nm is 1.73. Most organic binders have a low index (around 1.5). However, there exists a high-index polyimide [23] (dashed line) which has a suitable dispersion, since the index matches that of SrB₄O₇ at 685 nm and follows it closely for the other emission wavelengths. At the absorption wavelengths (< 600 nm), the index of the binder is higher than that of SrB₄O₇. Another option is mixing high-index nanoparticles in a binder to enhance its refractive index. In Fig. 3(b) we show how the index of a mixture of an organic binder (polyvinylpyrrolidone) and TiO₂ nanoparticles [24] depends on its composition. To match the index of SrB₄O₇ at 685 nm, a composition of 29 volume% TiO₂ is needed. The dispersion of this material is also shown in Fig. 3(a) (dotted line). At both lower and higher wavelengths, the index of this material is slightly less favorable than that of the polyimide.

It is not easy to make good layers of phosphor particles dispersed in a binder. All constituents should be compatible with each other and with the dispersant and it should be possible to easily apply them in a simple manner, such as by spin or blade coating. The layer should adhere to the light guide without cracking, so their thermal expansion coefficients should be similar. Moreover, the materials should be stable over time, even after prolonged irradiation by sunlight. In that respect, the combination of TiO₂ nanoparticles and an organic binder is dubious since TiO₂ is known to photocatalyze the decomposition of organic materials [25]. Finally, the binder should not absorb the incident or luminescent light. In that respect, polyimide is not very suitable as it absorbs UV and blue light. We were able to make thin layers (up to 20 μm) with reduced scatter. These layers remained stable for

approximately two weeks. Since the absorption length of our phosphor is around 30 μm , thicker layers are needed to obtain sufficient absorption.

Using such a layer, which absorbs approximately 50% of incident light at 500 nm wavelength, we made a first prototype device ($50 \times 50 \times 5 \text{ mm}^3$), using custom-made [26] silicon solar cells ($50 \times 5 \text{ mm}^2$). At 1 sun illumination, we measured a solar efficiency of approximately 15% that of a bare solar cell, slightly lower than that of an optimized demo containing an organic dye [27]. However, in the case of an inorganic phosphor, the non-converted sunlight that scatters towards the solar cell contributes more than half to the efficiency. Further research is needed to optimize the performance of this LSC configuration.

4. Cholesteric-liquid-crystal based filters

The escape of luminescent light can be prevented by applying wavelength-selective filters on top of the light guide. There exist a number of materials that may serve as filters, such as dielectric stacks and three-dimensional photonic crystals [28]. An interesting class of filters are cholesteric liquid crystals (CLCs), which act as Bragg reflectors for circularly polarized light. These materials are attractive, since they are self-aligning and can be produced over large areas [11]. It is possible to make broad-band filters by applying a pitch gradient in the cholesteric stack, exploiting the driving forces of a UV-intensity gradient across the film thickness and the different reactivity of a (right- or left-handed) chiral monomer and a nematic monomer [29]. Polarization-independent filters can be made either by combining two filters of opposite chirality or by combining two filters with the same chirality and a half-lambda wave plate [11].

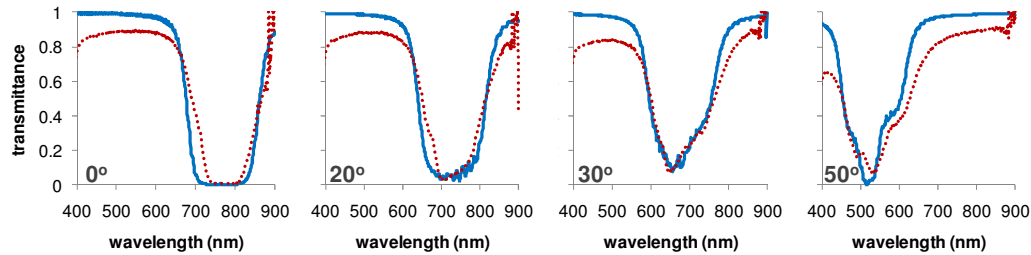


Fig. 4. Transmission spectra for various incident angles (in glass) of a right-handed CLC stacked on top of a left-handed CLC. The pitch varies linearly from 437 nm to 520 nm in the right-handed material and from 429 nm to 521 nm in the left-handed material, respectively. Dashed lines indicate the experiment, solid lines indicate simulated results.

Recently [12] we realised such filters aimed at reflection of luminescent radiation with a wavelength of approximately 700 nm. In Fig. 4, the transmission spectra for various angles are shown for a filter consisting of two CLCs with opposite chirality, each having a pitch gradient from 430 to 520 nm. The results for a stack of two CLCs with the same chirality and a half-lambda wave plate in between are similar. There is good agreement between experimental results and simulations using a known method [30] to calculate the propagation of electromagnetic waves in a stack of wave plates.

The calculated angular and wavelength dependence of the reflectivity of such a filter is plotted in Fig. 5(a). Note that the reflection band shifts to lower wavelength for larger angles of incidence according to Bragg's law, which for the low- and high-wavelength edges of the reflection band can be written as $\lambda_{1,2} = n_{o,e} p_{1,2} \cos \theta_{in}$, where n_o and n_e are the ordinary and extraordinary refractive indices of the liquid crystal, p_1 and p_2 are the smallest and largest pitch, respectively, and θ_{in} is the incident angle inside the filter material. This implies that, for high incident angles, the incoming sunlight will be reflected and hence be prevented from entering the light guide and from being absorbed by the luminophore. As will be shown in the next Section, this detrimental effect can be as large as the advantageous effect on the luminescent radiation.

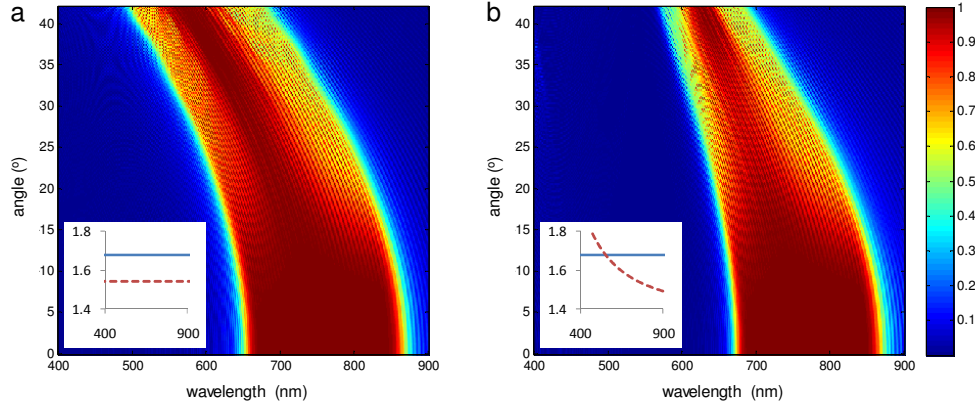


Fig. 5. Calculated reflectivity as a function of wavelength and (internal) angle of incidence for (a) no dispersion and (b) special dispersion. The dispersion of n_e (solid line) and n_o (dashed) are shown in the insets.

Hence, a filter which does not have this angular dependence would be desired. In principle, this is possible with a suitable wavelength dependence of the constituent materials of the filter. If, in case of a CLC, the dispersion is such that $n_o = n_e$ at a certain wavelength, the reflection band will vanish at that wavelength. This is shown in Fig. 5(b), where a material is used with dispersion as indicated in the inset. We assume that the difference between the two refractive indices decreases with decreasing wavelength and vanishes at 550 nm. Indeed, the calculation shows no reflection below this wavelength. In the next Section the effect of such filters on LSC performance will be quantified. One may wonder whether it is possible to realize such a filter in practice. Most materials exhibit a dispersion that is larger when the refractive index is larger. However, liquid crystals may have a larger dispersion [31] of n_o than of n_e while $n_e > n_o$. Although their properties may not be as favorable as those of Fig. 5(b), it should be possible to realize filters with less angular dependence than that of Fig. 5(a).

5. Simulation results

Simulations were performed using LightTools [32] ray-tracing software. For the light guide, we define a plate with refractive index $n = 1.5$ (and negligible absorption) and dimensions $100 \times 100 \times 2.5 \text{ mm}^3$ (unless stated otherwise). The luminophore is applied as a $100 \text{ }\mu\text{m}$ thick coating at the bottom of the light guide. The bottom side of the coating is a perfect mirror (100% reflectivity for all angles). The top surface of the light guide may be covered by a wavelength-selective filter. The incident radiation has a Lambertian distribution, hitting the top surface from all directions. The four sides of the light guide are covered with receivers. We will consider the collection probability p of the concentrator, that is, the ratio between the number of photons collected by the receivers and the total number of incident photons. This is related to the concentration factor as $c = p G$, where the geometric gain G is the ratio between the area of the concentrator on which the light impinges and that of the receivers. For the chosen configuration, $G = 10$.

First we performed model simulations with an idealized phosphor. The absorption spectrum is approximated by a constant spectrum between 300 and 600 nm with an absorption length of $30 \text{ }\mu\text{m}$ (enough to guarantee 99.9% absorption). As an approximation of the emission spectrum, we took a single emission line at 700 nm. The absorption length for the emitted radiation can be varied, as well as the QE of the phosphor. Various kinds of filters can be applied. The idealized filters have a square reflection band. For the incident spectrum, we take the solar (AM1.5G) spectrum between 300 and 600 nm. The other, non-absorbing, part of the solar spectrum has to be taken into account to calculate the total efficiency. If the photovoltaic cell is made of crystalline silicon, 30.3% of the AM1.5G solar photon flux up to the absorption edge (1100 nm) is taken into account; for GaAs (absorption edge 870 nm), this

number is 41.4%. So (neglecting scattering of radiation towards the photovoltaic cells), the collection probabilities should be multiplied by these numbers to obtain the total collection probabilities. To obtain the efficiency of the total system, in good approximation the efficiency of the bare photovoltaic cell can be multiplied by this total collection probability.

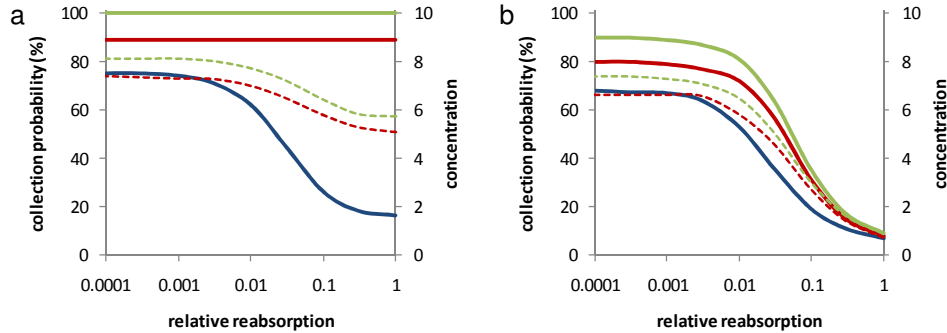


Fig. 6. Collection probability and concentration vs. relative reabsorption in an LSC. From top to bottom: with filter with special dispersion and 100% reflectivity, with filter with normal dispersion and 100% reflectivity, with filter with special dispersion and 90% reflectivity (dashed), with filter with normal dispersion and 90% reflectivity (dashed), without filter. (a) QE = 100%, (b) QE = 90%.

In Fig. 6, the effect of a variation of reabsorption on collection probability and concentration is shown. The relative reabsorption is defined as the ratio between the absorption length for the emitted radiation and that of the incident absorbed radiation. Figure 6(a) shows results for the case of QE = 100%. Without filter, the collection probability approaches the theoretical value of $(1 - n^{-2})^{1/2} = 75\%$ (for $n = 1.5$) at small reabsorption and decreases with increasing reabsorption. With filter, the collection probability does not depend on reabsorption, but is constant at 89% for a filter with normal dispersion (as in Fig. 5(a), inset) that reflects the luminescent light above 680 nm. The source of the missing 11% is the part of the incident solar spectrum that is blocked by the filter at high angles. With special dispersion (like in Fig. 5(b), inset), the sunlight is not blocked and 100% collection probability is reached. In addition, data for filters with 90% reflectivity are shown (dashed lines), in which the collection probability is reduced. The reason that the collection probability decreases with increasing reabsorption is as follows: for large reabsorption, there will be a correspondingly large amount of reemitted radiation (if QE = 100%) but not all reemitted radiation will be reflected back if the reflectivity of the filter is below 100%. In the cases that QE is smaller than 100%, Fig. 6(b), both with and without filter, the collection probability decreases with increasing reabsorption. Note that, in the case of small to medium reabsorption, the use of a realistic filter (90% reflectivity) with normal dispersion gives no improvement of the collection probability. Only filters with special dispersion and/or a very high reflectivity will help in this case. If reabsorption is relatively high, less perfect filters are beneficial, but the attainable concentration is even lower.

Next, we consider the effect of scattering by the phosphor, present as phosphor particles in a binder. In the simulations, it is assumed that the scattering can be described by Mie theory [32]. We assume that the phosphor particles have a refractive index of 1.7, a diameter of 5 μm and that the density is 30 volume% (corresponding to 4.6×10^6 particles mm^{-3}). The results for the collection probability as a function of the difference in refractive index with the binder are shown in Fig. 7. Without luminescence (dotted line), the situation is as in Fig. 1(a): the concentration factor is low and increases with (absolute) difference in refractive index. With luminescence, the maximum concentration is reached for zero refractive-index difference. It is even higher than in Fig. 6, because guiding in the layer with index 1.7 is possible at higher angles than with index 1.5. The performance decreases with increasing (absolute) refractive-index difference, but a difference of a few hundredths still results in acceptable gains. The effect of filters is similar to the results seen in Fig. 6. With filter, a higher refractive-index

difference still leads to acceptable results. Also the effect of a QE smaller than 100%, Fig. 7(b), is similar to that discussed above, Fig. 6(b).

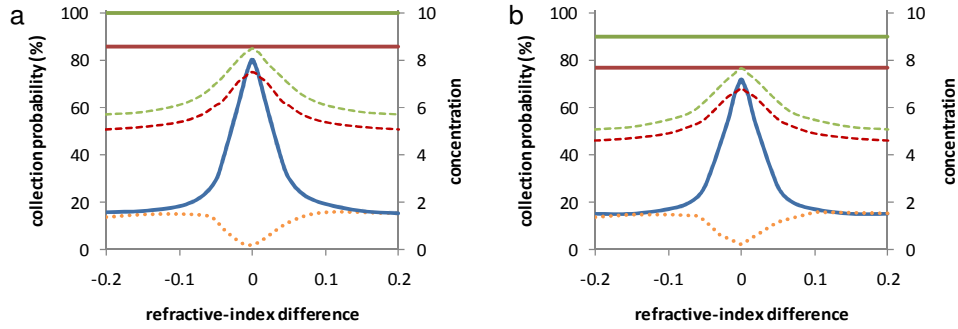


Fig. 7. Collection probability and concentration vs. difference in refractive index between scattering phosphor particles and binder. From top to bottom: with filter with special dispersion and 100% reflectivity, with filter with normal dispersion and 100% reflectivity, with filter with special dispersion and 90% reflectivity (dashed), with filter with normal dispersion and 90% reflectivity (dashed), without filter, only scattering particles (dotted).

(a) QE = 100%, (b) QE = 90%.

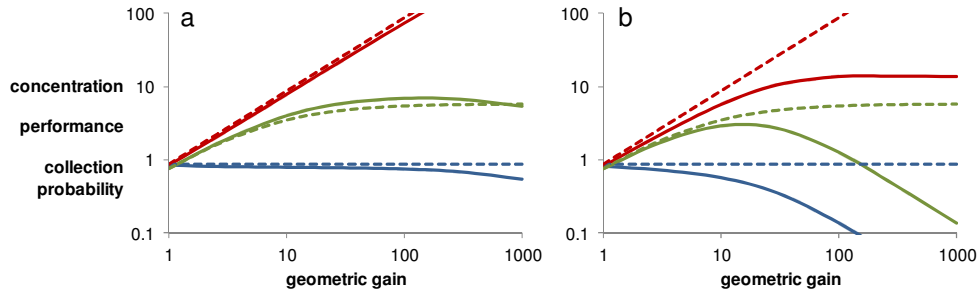


Fig. 8. (From top to bottom:) concentration, relative performance and collection probability vs. geometric gain in an LSC, without (solid line) and with (dashed) filter, for (a) matching phosphor ($n_{\text{binder}} = 1.7$) and (b) non-matching phosphor ($n_{\text{binder}} = 1.68$).

Furthermore, we investigate the effect of changing the size of the concentrator and hence the geometric gain G . We do this by varying the length of the concentrator plate from 10 mm to 10 m, while keeping the width equal to the length but maintaining the thickness at the value 2.5 mm. The phosphor layer consists of phosphor particles with refractive index 1.7 in a binder, for which we consider the cases with refractive index $n_{\text{binder}} = 1.7$ and $n_{\text{binder}} = 1.68$. The relative reabsorption is taken 0.0002. Figure 8 shows the results of the collection probability p , the concentration factor $C = pG$, as well as the relative performance r . Here we define the performance relative to that of a bare solar cell as the concentration per relative unit of costs $r = C/\$$. The relative costs can be written as $\$ = 1 + aG$, where a is the ratio between the costs per unit area of the light guide (including phosphor, mirrors and so on) and those of the solar cell. A reasonable number for a cost ratio is $a = 0.10$, for an LSC without a filter. The performance initially increases with geometric gain, but for larger geometric gains it then decreases. In case of an index-matching phosphor, Fig. 8(a), where both scattering and reabsorption are small, the decrease occurs for large values of G . In the non-matching case, Fig. 8(b), the relative performance reaches a maximum value close to 3 for G about 20. The behavior for a non-scattering phosphor with reabsorption is qualitatively similar. We also show data for the case with the filter with normal dispersion (for the filter with special dispersion, the values are approximately 12% higher), where we assume a cost ratio $a = 0.15$

for an LSC with cholesteric filter. It can be concluded that filters help to improve the performance in cases of significant scattering and/or reabsorption.

As was mentioned above, in these simulations only the incident solar spectrum up to 600 nm was taken into account. This implies that the calculated values for the collection probabilities, and hence also those for the concentration factor and relative performance, should be multiplied with a factor 0.303 for Si and 0.414 for GaAs-based solar cells. In fact, the calculated performance is relative to that using the same part of the spectrum (up to 600 nm) for the bare solar cells. Hence a combination of luminescent materials covering a larger part of the solar spectrum should be used to be more cost effective.

Finally, we performed simulations for a more realistic material, using the measured absorption and emission spectra for the Sm^{2+} -based phosphor (see Section 2) and $\text{QE} = 90\%$. The particle size and density are the same as described above. For the refractive index of the phosphor, we use that of SrB_4O_7 (Fig. 3(a), solid line); for the binder that of high-index polyimide (Fig. 3(a), dashed line). With this combination, the luminescent light will hardly scatter, whereas the path length of the incident sunlight in the phosphor is somewhat enhanced. For the light guide we take $n = 1.59$ (polycarbonate). As for the filters, we investigated both cases of Fig. 5. We found that the collection probability without filter is $p = 65\%$; with the normal filter of Fig. 5(a) it is $p = 62\%$; with the special filter of Fig. 5(b) it is $p = 70\%$. These results are similar to those of Fig. 7. The values are slightly lower than in Fig. 7(b), mainly because not all sunlight is absorbed in the absorption tail between 570 and 600 nm (again the solar spectrum up to 600 nm is used). Also in this case, a filter with special dispersion is needed to enhance the performance of the luminescent concentrator.

6. Discussion and conclusion

Luminescent solar concentrators have good prospects to provide inexpensive photovoltaic energy and, since they are made of colored sheets of material, they can be attractive objects to integrate in a built environment or consumer appliances. However, to make them work effectively, further improvements are required. First, luminescent materials are needed with high absorption, little reabsorption and high quantum efficiency. Our Sm^{2+} -based phosphor, with a relatively broad absorption spectrum and main emission peaks around 700 nm, fulfills most of these requirements. The problem with inorganic phosphors with particle size in the micrometer range is that they scatter the emitted light. In principle it is possible to solve this by using a refractive-index-matching binder, but it is still a challenge to make stable layers that absorb enough radiation and that do not scatter. The best prospects for high-index binders are for those based on stabilized nanoparticles [33]. The problem of escape by scattering, or by reabsorption followed by reemission, can be mitigated by the use of wavelength-selective filters. However, with normal filters, sunlight incident at high angles will be blocked because of the angular dependence of the reflection wavelength. This could be avoided by the use of special filters in which the reflection vanishes at short wavelengths as the result of negative birefringence dispersion. Simulations show that a significant fraction of the absorbed photons can be converted to luminescent photons that reach the photovoltaic cells. A main challenge is absorbing a significant portion of the solar spectrum. Although the proposed Sm^{2+} -based phosphor is better than other proposed materials, its absorption spectrum only covers 30% of the solar spectrum available for absorption by silicon solar cells (41% for GaAs). To realize the promises of the luminescent solar concentrator, a combination of luminescent materials covering larger fractions of the solar spectrum is required, together with the mentioned measures to avoid scatter, reabsorption and escape.

Acknowledgments

The authors would like to thank Kees Bastiaansen, Ties de Jong, Shufen Tsoi (Eindhoven University of Technology), Nick Christogiannis (Utrecht University), Daniëlle Beelen, Remco van Brakel, Sander de Brouwer, Hugo Cornelissen, Wouter Dekkers, Lieven Desmet, Merijn Giesbers, Willie Hardeman, Chi-Wen Lin, Arno Ras, Marc Verschuuren and Helmut Zahn (Philips Research) for their contributions and useful discussions. This work was partly

supported by SenterNovem (project IS073014), Stichting voor Technische Wetenschappen (VIDI grant 7940) and NanoNextNL (HTSM05 Energy).